Variation in Young's modulus along the length of a rat vibrissa

Brian W. Quist [a], Rafay A. Faruqi [a], Mitra J.Z. Hartmann [a,b],*

[a] Department of Biomedical Engineering, Northwestern University, Evanston, IL 60208, USA
[b] Department of Mechanical Engineering, Northwestern University, Evanston, IL 60208, USA

ARTICLE INFO

ABSTRACT

Rats use specialized tactile hairs on their snout, called vibrissae (whiskers), to explore their surroundings. Vibrissae have no sensors along their length, but instead transmit mechanical information to receptors embedded in the follicle at the vibrissa base. The transmission of mechanical information along the vibrissa, and thus the tactile information ultimately received by the nervous system, depends critically on the mechanical properties of the vibrissa. In particular, transmission depends on the bending stiffness of the vibrissa, defined as the product of the area moment of inertia and Young's modulus. To date, Young's modulus of the rat vibrissa has not been measured in a uniaxial tensile test. We performed tensile tests on 22 vibrissae cut into two halves: a tip-segment and a base-segment. The average Young's modulus across all segments was 3.34 ± 1.48 GPa. The average modulus of a tip-segment was 3.96 ± 1.60 GPa, and the average modulus of a base-segment was 2.90 ± 1.25 GPa. Thus, on average, tip-segments had a higher Young's modulus than base-segments. High-resolution images of vibrissae were taken to seek structural correlates of this trend. The fraction of the cross-sectional area occupied by the vibrissa cuticle was found to increase along the vibrissa length, and may be responsible for the increase in Young's modulus near the tip.

© 2011 Published by Elsevier Ltd.

1. Introduction

The rat vibrissal (whisker) system is an increasingly important model in the field of neuroscience for the study of the sense of touch (Diamond et al., 2008). Rats actively tap and sweep their vibrissae against objects to extract detailed spatial features such as orientation (Polley et al., 2005) and texture (Jadhav and Feldman, 2010).

Unlike the antennae of insects (Staudacher et al., 2005), vibrissae have no sensors along their length. Instead, all mechanical information must be transmitted along the vibrissa length to the receptors located in the follicle at the vibrissa base. Thus, the mechanical properties of the vibrissa determine how the contact with the environment is transmitted to the nervous system.

The transmission of mechanosensory information will depend critically on the bending stiffness of the vibrissa (Birdwell et al., 2007; Solomon and Hartmann, 2006), defined as the product of the area moment of inertia and Young's modulus (Hibbeler, 2011). The area moment of inertia can be found from vibrissa geometry; in contrast, it requires significantly more effort to determine Young's modulus.

Young's modulus of a rat vibrissa was measured previously using nano-indentation techniques (Herzog et al., 2005), but this study was limited to a single sample, and it is difficult to exclude the possibility that the non-uniform strain directly below the indenter caused inelastic deformation. Young's modulus of the vibrissa has also been inferred from matching experimental data with linear elastic models of bending and/or resonance (Birdwell et al. 2007; Hartmann et al. 2003; Neimark et al. 2003). Both of these types of tests, however, require elastic solutions to interpret the results. Resonance experiments additionally rely on measuring dynamic elastic properties, which are often different from static ones.

The tensile test is generally the simplest and most easily interpreted method for determining Young's modulus. The tensile test fundamentally requires only the definition of stress as force/area and strain as a ratio of lengths. To date, however, Young's modulus has not been determined using a uniaxial tensile test.

The present study performs uniaxial tensile tests to quantify Young's modulus of rat vibrissae. We show that Young's modulus is larger near the vibrissa tip than near the base. High-resolution images of vibrissae showed that the area fraction occupied by the vibrissa cuticle increased along the vibrissa length, and therefore is likely to be the physical characteristic that underlies this variation in Young's modulus.

Accurate values of Young's modulus will be important in validating models of vibrissa deformation used to predict sensory input to the vibrissal–trigeminal pathway.

Methods

All procedures were approved in advance by the Northwestern Animal Care and Use Committee. Two different sets of vibrissae were used for mechanical testing and image analysis.

* Corresponding author. Mechanical Engineering Department, Northwestern University, 2145 Sheridan Road, Evanston, IL 60208, USA. Tel.: +847 467 7288; fax: 847 491 4928.

E-mail address: m-hartmann@northwestern.edu (M.J.Z. Hartmann).

1.1. Vibrissa acquisition for mechanical experiments

We mechanically tested 22 vibrissae plucked from two female Sprague Dawley rats briefly anesthetized with isoflurane. Rats were approximately six months old and weighed between ∼350 and ∼360 g. A matched right/left pair of vibrissae (e.g., the right and left C1 vibrissae) was obtained using jeweler's tweezers to pull each vibrissa out of the follicle. Only two vibrissae were removed at a time to ensure that testing was performed within 24 h. The vibrissae tested were: alpha, beta, gamma, delta, C1, and C2.

Each vibrissa was cut into half with a razor blade to yield two samples for mechanical testing: a tip-segment and a base-segment. Each segment was trimmed to an approximate length of 15 mm ($\pm$ ∼7 mm from the segment center). Finally, both ends of the segment (∼2 mm at each end) were flattened between two hard surfaces to permit the segment to be mounted for testing (see Supplementary Material Part I).

1.2. Mechanical testing

Uniaxial loading tests of each vibrissa segment were performed using the mechanical setup schematized in Fig. 1A. The setup had four components: a precision linear actuator (Mach-1, Biosyntech Inc.), a 1 kg single-axis load cell (Biosyntech Inc.), custom-designed clamping mechanisms (top and bottom), and the mounted vibrissa sample. A photograph of the side-view of the setup is shown in Fig. 1B.

To provide a gripping surface for the clamps of the micromechanical tester, and ensure that the sample was precisely aligned with the direction of the applied load, each vibrissa sample was mounted across two thin aluminum plates (thickness 0.02 in, 9536K18, McMaster-Carr). Further details on mechanical testing are provided in Supplementary Material Part II.

All samples were strained at a rate of 10 µm/s. This value was chosen to be within the range typically used when studying keratin materials, between 5.5–833 µm/s (Bonser and Purslow, 1995; Kania et al., 2009; Li et al., 2010; Thozhur et al., 2006; Tombolato et al., 2010). Only one of these studies examined how Young's modulus varied with strain rate; the effect was generally small. For example, in a study of human beard hair, Thozhur et al. found a 6% increase in Young's modulus when the strain rate was changed by an order of magnitude (8.3 um/s to 83 um/s). Thus, because our strain rate was at the lower end of the typical ranges, our results will tend to represent a lower bound. We expect the final value of Young's modulus to increase by only ∼6% if strain rate were increased up to a factor of ten.

The Mach-1 linear actuator had a range of 10 cm with a resolution of 1.5 µm. Samples were not typically tested until rupture, but the test did reach the inelastic region of deformation (Results, Fig. 3). The output of the Mach-1 load cell was in terms of grams, which was multiplied by a factor of $9.8\ \mathrm{ms}^{-2}$ to obtain force in millinewtons (mN).

Relative humidity and temperature at the time of sample preparation and testing were recorded. The temperature was approximately constant at $72.7 \pm 0.5\ ^\circ$F. The relative humidity was also approximately constant at $17.6 \pm 1.9\%$. Further considerations for the experimental design are provided in Supplementary Material Part III.

1.3. Analysis of mechanical data

The force and displacement measurements obtained from the micromechanical tester were used to generate a stress–strain curve for each sample, which was then used to find Young's modulus. Stress and strain calculations were performed only for the portion of the vibrissa that was exposed between the epoxied regions.

Young's modulus was calculated as the slope of the linear region of the plot of stress versus strain (Results, Fig. 3). To determine the linear region, we first performed a linear fit that included only the first ten points in the curve and found the standard error of the estimate. We then increased the number of points included in the fit one by one, and calculated the standard error of the estimate for each fit. The linear region was taken to include those points that were fit with the smallest standard error of the estimate.

1.4. High-resolution image acquisition and analysis

Select vibrissae were plucked from four female Sprague Dawley rats. The rats were 5 months old and weighed ∼300 g. Before vibrissa plucking, each rat was anesthetized with an intraperitoneal injection of a 1 ml mixture of ketamine hydrochloride (25 mg/ml), xylazine HCl (1.25 mg/ml), and acepromazine maleate (0.25 mg/ml).

20 vibrissae were used in the final image analysis. These vibrissae were: alpha ($n=3$), A1 ($n=2$), A4 ($n=1$), beta ($n=1$), B1 ($n=1$), B2 ($n=4$), B3 ($n=1$), B4 ($n=1$), C1 ($n=1$), C2 ($n=1$), C3 ($n=3$), and E3 ($n=1$).

Each vibrissa was mounted on a standard microscope slide (25 mm × 75 mm, 12-544-4, Fisher Scientific) using an aqueous-based mounting medium (SHUR/Mount 17992-01, Electron Microscopy Sciences). Samples were covered with a coverslip (24 mm × 50 mm, 12-543D, Fisher Scientific), taking care to purge as many air bubbles as possible without moving the vibrissa. This assembly was then allowed to dry overnight. Finally, the coverslip was sealed with an acrylic nail polish for long-term storage and imaging.

The slides of the vibrissae were imaged on a microscope fitted with a 10x objective, a digital camera, and an actuated stage. Custom written software in Python was used to acquire a series of tiled images that spanned the entire vibrissa length. To image a slide, the user first traced the shape of the vibrissa. The program then controlled the focus, the xy-stage position, and the camera and retraced the vibrissa in successive passes. An example of the output is shown in Fig. 2 for images taken at five different locations along the vibrissa length. Some small air bubbles (dark and bright circles) remained in the slides despite efforts to remove them during the fixing process.

The set of images associated with a vibrissa were tiled together within Matlab. Each composite vibrissa was visually inspected to confirm accurate tiling and the user then clicked on ten points to identify the approximate contour of the vibrissa. These selected points were linearly interpolated to provide an estimate of the overall vibrissa shape.

Analysis of the composite image was performed in 10-pixel increments ("steps") along the user-selected vibrissa contour. At each step, a vector normal to the user-selected vibrissa contour line was computed and a cross-section of the vibrissa found by selecting a fixed number of pixels above and below the contour line. Within each cross-section, the outer and inner boundaries of the top and bottom cuticles were
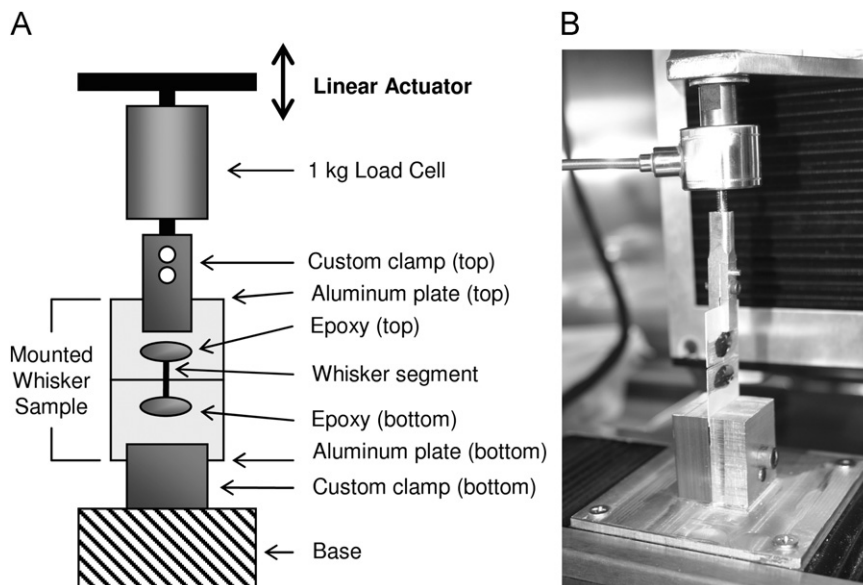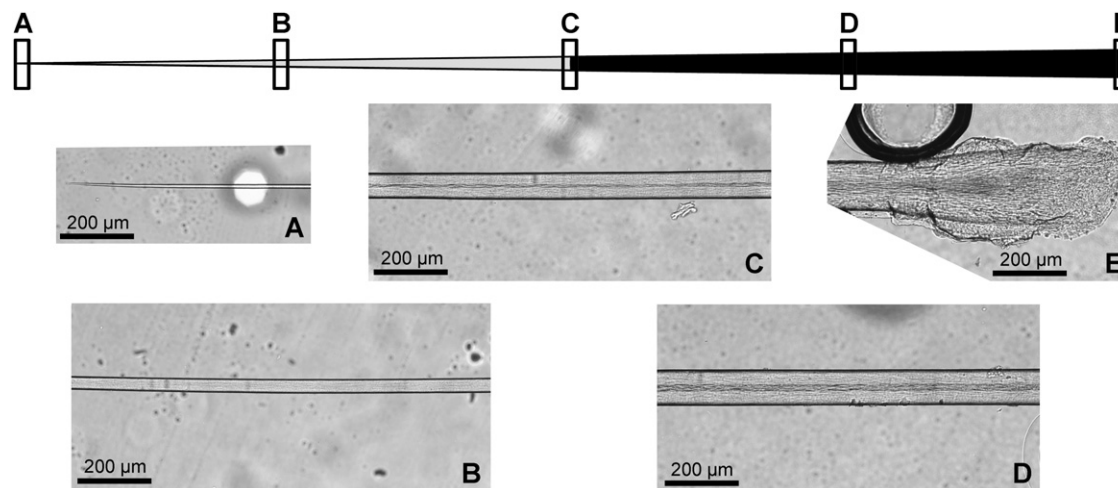

Fig. 1. Micromechanical testing setup. (A) Front-view schematic of the setup (not to scale). (B) Photograph of the side-view of the setup with a mounted vibrissa sample.

Fig. 2. Examples of high-resolution images obtained from five different regions of a C3 vibrissa. This vibrissa required 38 images to capture its entire length. All images have been cropped from their original size of 1600 × 1200 pixels. Images show the (A) tip, (B) segment along the distal half of the vibrissa length, (C) segment at the center of the vibrissa, (D) segment along the proximal half of the vibrissa length, and (E) base.
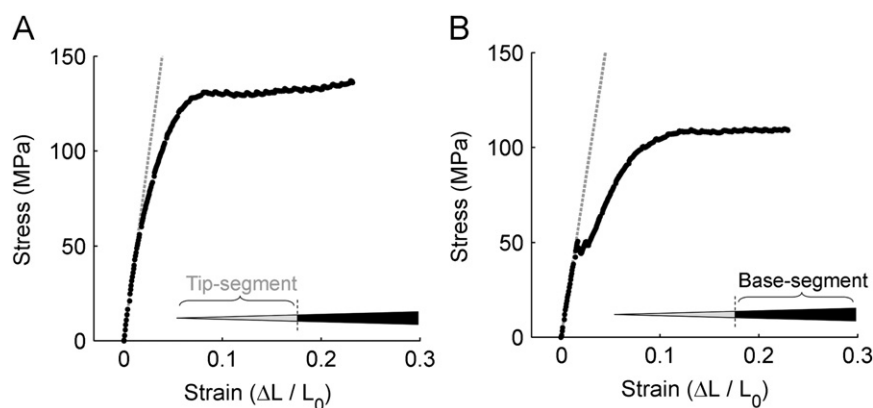
Fig. 3. Stress–strain curves for tip and base segments of a delta vibrissa. In both subplots, black points correspond to the complete uniaxial loading trial. Dashed gray lines indicate the fit to the linear region of the data.

found. Subtracting the two outer boundaries yielded the diameter of the vibrissa. The cuticle thickness for the cross-section was the average of the top and bottom cuticle thicknesses. The outer-most boundaries of the vibrissa were centered at each step to generate a "straight" vibrissa as shown in Figs. 2 and 5.

2. Results

2.1. Stress–strain curves from tip and base segments of the same vibrissa

Fig. 3 shows stress–strain curves obtained for the tip-segment and the base-segment of the same delta vibrissa. Experimental data from the tip-segment (Fig. 3A) reaches a maximum stress of 137 MPa, while the base-segment reaches a maximum stress of 110 MPa (Fig. 3B). The slope of the linear region of the stress strain curve represents Young's modulus, and was found to be 3.83 GPa for the tip-segment and 3.34 GPa for the base-segment.

2.2. Young's modulus is about 4 GPa near the vibrissa tip, and about 3 GPa near the vibrissa base

The average value of Young's modulus across all samples was 3.34 ± 1.48 GPa, as illustrated in Fig. 4A. Young's modulus did not strongly depend on the diameter of the vibrissa sample (ANOVA, $p=0.19$). However, the average value of Young's modulus for tip-segments was larger than the average value of Young's modulus for base-segments: 3.96 ± 1.60 GPa and 2.90 ± 1.25 GPa, respectively. Thus, Young's modulus was strongly correlated with segment identity (ANOVA, $p=0.03$).

Next, we tested whether Young's modulus varies within a vibrissa, rather than just by population averages. This analysis indicates whether the trend for base-segments to have a lower Young's modulus holds within each vibrissa, or if some vibrissae just have a lower Young's modulus overall. Fig. 4B plots Young's modulus versus segment identity (tip or base) for the same vibrissa. Fourteen of the 22 vibrissae provided data for both tip and base segments. All but three of the 14 vibrissae had a larger value of Young's modulus for the tip-segment than for the base-segment (two-sided paired t-test, $p=0.02$).

Importantly, Young's modulus was not correlated with either vibrissa row (ANOVA, $p=0.30$) or column (ANOVA, $p=0.59$). This suggests that Young's modulus is independent of the position in the array from where the vibrissa was taken.

Our experimental values for Young's modulus exhibited considerable scatter, likely because vibrissae are not structurally homogeneous. As we will subsequently show, there is considerable variability in the cuticle thickness of each vibrissa and the relative areas occupied by the vibrissa cuticle and cortex.
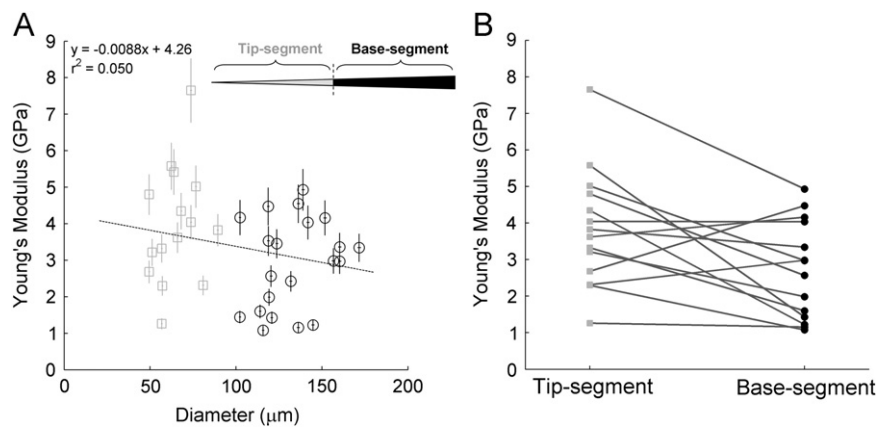
Fig. 4. Variation of Young's modulus with segment diameter and segment identity: (A) Young's modulus versus diameter of the vibrissa sample. Error bars were obtained using error propagation, resulting in standard deviations equal to 11.5% of the measured Young's modulus. A linear fit to the data is indicated with the dotted line and equation. (B) Young's modulus was larger at the tip than at the base for 11/14 vibrissae. Lines connect the value found for the tip-segment to the value found for the base-segment.
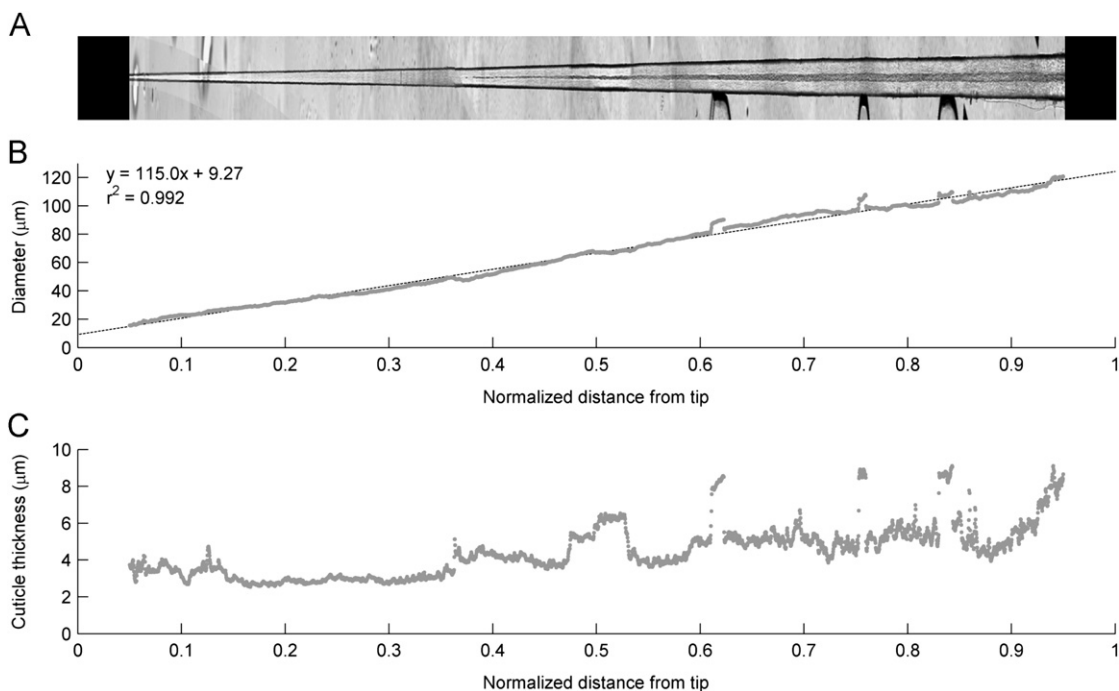
Fig. 5. The C3 vibrissa ("straightened" via image processing) is shown with corresponding measurements of diameter and cuticle thickness. (A) C3 vibrissa from Fig. 2. The first 5% and last 5% of the vibrissa are omitted to simplify image processing. (B) Vibrissa diameter varies linearly with distance from the tip of the vibrissa. Distance has been normalized to the total length of the vibrissa. A linear fit is shown as a gray line. (C) Cuticle thickness versus normalized distance from the vibrissa tip.

We measured two environmental factors (humidity, ambient temperature) to control for external influences on the measurement of Young's modulus. Young's modulus was not statistically correlated with either temperature or humidity at the time of testing (ANOVA, $p=0.25$ for temperature, $p=0.92$ for humidity). The order in which the segments from a single vibrissa were tested (base or tip segment first) was randomized, and the overall sequence order was not statistically correlated with Young's modulus (ANOVA, $p=0.40$). Finally, Young's modulus was not correlated with the taper of the vibrissa along the exposed vibrissa segment (ANOVA, $p=0.70$).

2.3. Three structural features vary with position along the vibrissa

We next looked for structural features of the vibrissa that could help explain the variation of Young's modulus. Fig. 5A illustrates the

C3 vibrissa after image processing (see Methods). This is the same vibrissa as shown in Fig. 2. The figure clearly illustrates three different regions of the vibrissa: the cuticle, seen as thick black edges; the cortex, seen as light gray between the cuticle; and the medulla, seen as the dark gray region in middle of the cortex.

Three characteristic geometric features are also observed clearly in this image of the vibrissa.

First, as described in previous studies (Ibrahim and Wright, 1975; Williams and Kramer, 2010), the diameter of the vibrissa tapers linearly with arc length. Fig. 5B illustrates the particularly strong linearity of this relationship for the C3 vibrissa.

Second, the medulla tapers from base to tip, and disappears for the distal half of the vibrissa. Previous studies have shown that the vibrissa medulla is mostly hollow, especially the most proximal regions (Carl et al., 2011). The medulla could therefore serve to decrease Young's modulus measured near the vibrissa base.
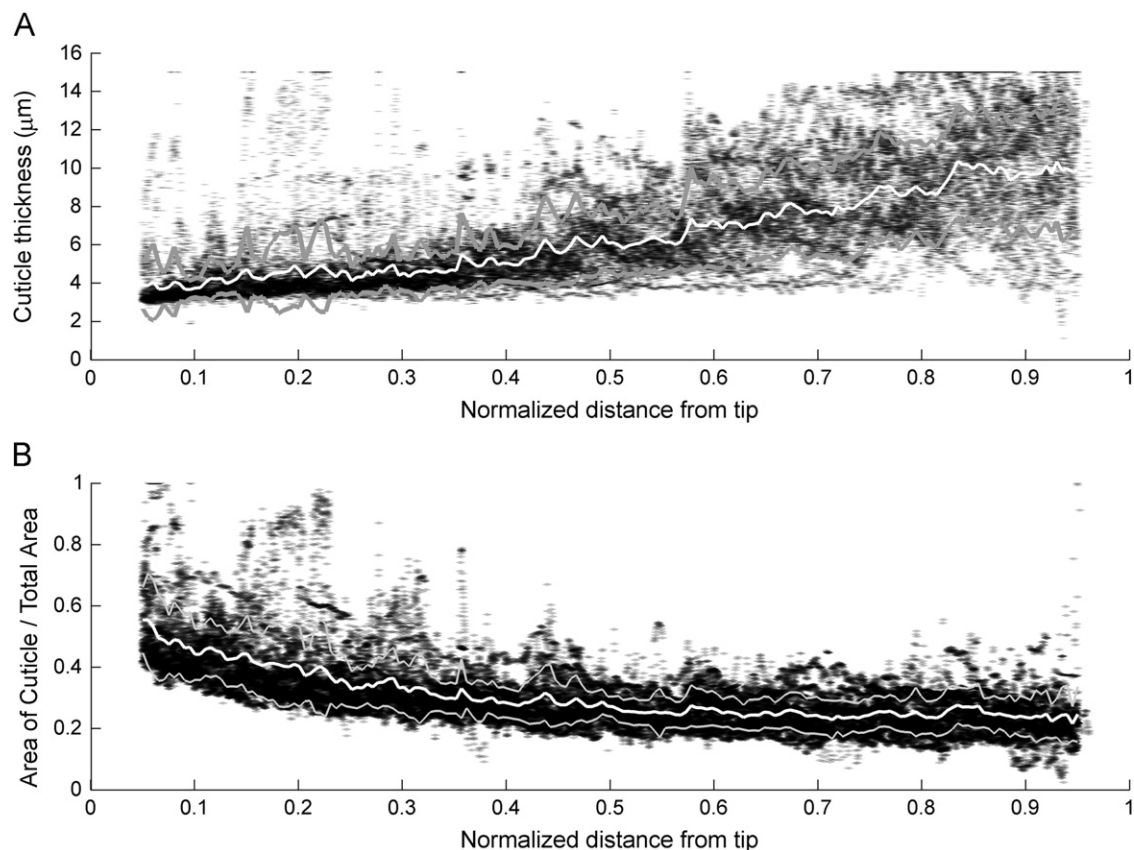
Fig. 6. Cuticle thickness and the fractional area of the cuticle versus distance along the vibrissa. (A) Cuticle thickness (averaged across the two sides of the vibrissa) is plotted as a function of the distance from the tip of the vibrissa. Distance is normalized to the total length of the vibrissa. (B) Area fraction of the cuticle. For (A) and (B), each data point is plotted as light gray, so that the overlapping data points become darker. The length of each data point on the x-axis represents a normalized distance from the tip of 0.005. Lines indicate the average (white) and standard deviation (light gray) for the dataset.

Third, the cuticle decreases in thickness from base to tip. Fig. 5C illustrates the measurement of cuticle thickness for the C3 vibrissa. We examined this feature in more detail by quantifying the cuticle thickness as a fraction of diameter for all 20 vibrissae.

2.4. The fractional area of the vibrissa occupied by the cuticle increases from base to tip

All vibrissae had cuticles that were thicker at the base than at the tip. Fig. 6A plots cuticle thickness as a function of distance from the tip for all 20 vibrissae. After averaging, it is immediately apparent that cuticle thickness is essentially constant near the tip (up until about 30–40%), while at distances further from the tip the cuticle thickens much more rapidly.

We performed a segmented linear analysis (Julious, 2001) to determine the change point between linear fits to the distal and proximal regions of the vibrissa. The analysis found a significant change in slope occurring at 0.371 ($p < 0.001$).

Importantly, however, although the cuticle thickness decreases from base to tip, the fractional cross-sectional area of the vibrissa occupied by the cuticle increases from base to tip (see Fig. 6B). This increase in the fractional area occupied by the cuticle is likely to be responsible for the increase in Young's modulus along the vibrissa length.

3. Discussion

The present study is the first quantification of Young's modulus of a vibrissa via a uniaxial tensile test. The average Young's modulus

across all segments was 3.34 ± 1.48 GPa. The average modulus of a tip-segment was 3.96 ± 1.60 GPa, while the average modulus of a base-segment was 2.90 ± 1.25 GPa.

3.1. Young's modulus of a vibrissa compared to that of other biological materials

Keratin is classified into two major groups based on wide-angle X-ray diffraction: α-keratin and β-keratin (Fraser and Macrae, 1980). α-keratin is associated with terrestrial mammals, and is found in skin, hair, hooves, and horns. β-keratin is associated with birds and reptiles and is found in beaks, feathers, and claws.

Typical Young's modulus values for low relative humidity α-keratin structure vary considerably, but are usually near 2–3 GPa. Specific values include: 2.20 GPa for bighorn sheep horns (Tombolato et al., 2010); 2.34 GPa for horns from domestic cattle (Li et al., 2010); 2.25–2.5 GPa for hair from a horse's mane (Kania et al., 2009); and 1.19–1.25 GPa for merino wool (Gibson et al., 2001). Horses' hooves deviate significantly from this trend, with a Young's modulus of ~14.6 GPa at 0% relative humidity (Bertram and Gosline, 1987).

The typical values for low relative humidity Young's modulus from β-keratin have a similar range to α-keratin structures: 2.25 GPa averaged across eight species of bird feathers (Bonser and Purslow, 1995); 1.74 GPa for feathers from genoo penguins (Bonser and Dawson, 2000); 2.07 GPa for duck down feathers (Bonser and Farrent, 2001); 3.66 GPa for ostrich feather (Taylor et al., 2004); and 2.7 GPa for ostrich claw (Taylor et al., 2004).
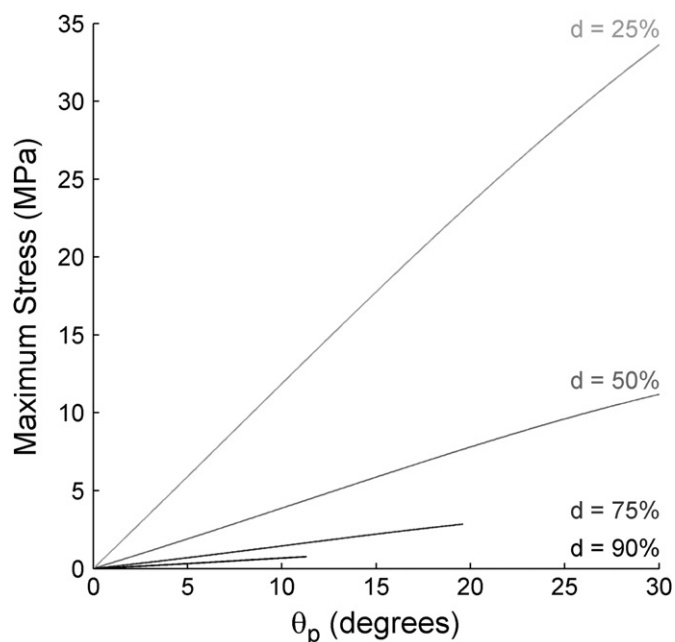
Fig. 7. Maximum stress at the vibrissa base during rotation into a point object placed at 25%, 50%, 75%, and 90% of the vibrissa length. The simulation assumes parameters typical of a delta vibrissa. Vibrissa length was set to 53.1 mm (Towal et al., 2011); diameter was set to 212 μm; taper ratio (base diameter divided by tip diameter) was set to 15 (Williams and Kramer, 2010); curvature was defined by a parabola with a quadratic coefficient of 0.0117 mm^{-1} (Towal et al., 2011); and Young's modulus was set to 3.34 GPa. Maximum stress is plotted versus the angle of rotation against a point-object, called theta-push, θ_p. Vibrissa was oriented to collide with its concave face towards the object. Lines terminate when the simulation became unstable.

The results of these studies are all consistent with the present finding that Young's modulus of rat vibrissae is near 3–4 GPa. Using nano-indentation techniques, Herzog et al. (Herzog et al., 2005) found a similar range of 1.3–3.9 GPa. Several previous studies of the rat vibrissa have calculated Young's modulus by leaving it as a free parameter when matching experimental data with linear elastic models of resonance and/or bending. These studies found values of 3.02–3.68 GPa (Hartmann et al., 2003), 7.8 GPa (Neimark et al., 2003), 3.5 GPa (Solomon and Hartmann, 2006), and 1.4–6.25 GPa (Birdwell et al., 2007).

3.2. Variation in the area fraction of the cuticle along the vibrissa length is likely responsible for variation in Young's modulus

Changes in Young's modulus along the length of the vibrissa must have a structural (material) correlate. Although the present study does not directly correlate the area fraction of the vibrissa cuticle with Young's modulus at different locations along the vibrissa, it demonstrates that both parameters increase from base to tip. Given that the cuticle is stiffer than the cortex (Parbhu et al., 1999), an increase in the fractional area of the cuticle is the most plausible structural correlate to the increase in Young's modulus near the vibrissa tip.

Intriguingly, the change-point for the cuticle thickness was located approximately 60–70% out along the vibrissa length (Fig. 6). This location coincides with the location at which the vibrissa tends to curve out of the plane (Knutsen et al., 2008; Towal et al., 2011).

3.3. Implications for whisking behavior

For a given diameter, increasing Young's modulus will produce larger reaction moments and forces. The finding that Young's

modulus is larger near the tip than near the base means that the tip region of the vibrissa is more stiff than would be predicted from the assumption of a constant Young's modulus.

Fig. 7 illustrates the results of a simulation that calculates the maximum bending stress that will occur at the vibrissa base as the vibrissa rotates against a point object placed at different locations along its length. The maximum bending stress is equal to the bending moment multiplied by the radius of the vibrissa divided by the area moment of inertia (Hibbeler, 2011). Even a large rotation of 30° against an object placed 25% along the vibrissa length results in a peak stress of only ~35 MPa. Given that the inelastic deformation does not occur until after approximately 100 MPa (Fig. 3), typical vibrissa deflections during the behavior remain well within the linear elastic region.

Conflict of interest statement

The authors do not have any conflicts of interest.

Appendix A. Supplementary material

Supplementary data associated with this article can be found in the online version at doi:10.1016/j.jbiomech.2011.08.027.

References

Bertram, J.E., Gosline, J.M., 1987. Functional design of horse hoof keratin: the modulation of mechanical properties through hydration effects. Journal of Experimental Biology 130 (1), 121–136.

Birdwell, J.A., Solomon, J.H., Thajchayapong, M., Taylor, M.A., Cheely, M., Towal, R.B., Conradt, J., Hartmann, M.J., 2007. Biomechanical models for radial distance determination by the rat vibrissal system. Journal of Neurophysiology 98 (4), 2439–2455.

Bonser, R., Purslow, P., 1995. The Young's modulus of feather keratin. Journal of Experimental Biology 198 (4), 1029–1033.

Bonser, R.H.C., Dawson, C., 2000. The mechanical properties of down feathers from gentoo penguins (Pygoscelis papua). Journal of Zoology 251 (04), 535–547.

Bonser, R.H.C., Farrent, J.W., 2001. Influence of hydration on the mechanical performance of duck down feathers. British Poultry Science 42 (2), 271–273.

Carl, K., Hild, W., Mampel, J., Schilling, C., Uhlig, R., Witte, H., 2011. Characterisation of statical properties of rat's whisker system. Sensors Journal, IEEE PP 99 1-1.

Diamond, M.E., von Heimendahl, M., Knutsen, P.M., Kleinfeld, D., Ahissar, E., 2008. 'Where' and 'what' in the whisker sensorimotor system. Nature Reviews Neuroscience 9 (8), 601–612.

Fraser, R.D., Macrae, T.P., 1980. Molecular structure and mechanical properties of keratins. Symposia of the Society for Experimental Biology 34, 211–246.

Gibson, C.T., Myhra, S., Watson, G.S., Huson, M.G., Pham, D.K., Turner, P.S., 2001. Effects of aqueous exposure on the mechanical properties of wool fibers—analysis by atomic force microscopy. Textile Research Journal 71 (7), 573–581.

Hartmann, M.J., Johnson, N.J., Towal, R.B., Assad, C., 2003. Mechanical characteristics of rat vibrissae: resonant frequencies and damping in isolated whiskers and in the awake behaving animal. Journal of Neuroscience 23 (16), 6510–6519.

Herzog, E.K., Bahr, D.F., Richards, C.D., Richards, R.F., Rector, D.M., 2005. Spatially dependent mechanical properties of rat whiskers for tactile sensing. Mechanical Properties of Bioinspired and Biological Materials 844, 119–123.

Hibbeler, R.C., 2011. Mechanics of Materials. Prentice Hall, Upper Saddle River, NJ, Pearson.

Ibrahim, L., Wright, E.A., 1975. Growth of rats and mice vibrissae under normal and some abnormal conditions. Journal of Embryology and Experimental Morphology 33, 831–844 (JUL):.

Jadhav, S.P., Feldman, D.E., 2010. Texture coding in the whisker system. Current Opinion in Neurobiology 20 (3), 313–318.

Julious, S.A., 2001. Inference and Estimation in a changepoint regression problem. Journal of the Royal Statistical Society: Series D (The Statistician) 50 (1), 51–61.

Kania, M., Mikolajewska, D., Marycz, K., Kobielarz, M., 2009. Effect of diet on mechanical properties of horse's hair. Acta of Bioengineering and Biomechanics 11 (3), 53–57.

Knutsen, P.M., Biess, A., Ahissar, E., 2008. Vibrissal kinematics in 3D: tight coupling of azimuth, elevation, and torsion across different whisking modes. Neuron 59, 35–42.

Li, B.W., Zhao, H.P., Feng, X.Q., Guo, W.W., Shan, S.C., 2010. Experimental study on the mechanical properties of the horn sheaths from cattle. The Journal of Experimental Biology 213 (3), 479–486.

Neimark, M.A., Andermann, M.L., Hopfield, J.J., Moore, C.I., 2003. Vibrissa resonance as a transduction mechanism for tactile encoding. Journal of Neuroscience 23 (16), 6499–6509.

Parbhu, A.N., Bryson, W.G., Lal, R., 1999. Disulfide bonds in the outer layer of keratin fibers confer higher mechanical rigidity: correlative nano-indentation and elasticity measurement with an AFM. Biochemistry 38 (36), 11755–11761.

Polley, D.B., Rickert, J.L., Frostig, R.D., 2005. Whisker-based discrimination of object orientation determined with a rapid training paradigm. Neurobiology of Learning and Memory 83 (2), 134–142.

Solomon, J.H., Hartmann, M.J.Z., 2006. Biomechanics: robotic whiskers used to sense features. Nature 443 (7111), 525.

Staudacher, E.M., Gebhardt, M., Durr, V., 2005. Antennal movements and mechanoreception: neurobiology of active tactile sensors. Advances in Insect Physiology 32 (32), 49–205.

Taylor, A.M., Bonser, R.H.C., Farrent, J.W., 2004. The influence of hydration on the tensile and compressive properties of avian keratinous tissues. Journal of Materials Science 39 (3), 939–942.

Thozhur, S., Crocombe, A., Smith, P., Cowley, K., Mullier, N., 2006. Structural characteristics and mechanical behaviour of beard hair. Journal of Materials Science 41 (4), 1109–1121.

Tombolato, L., Novitskaya, E.E., Chen, P.-Y., Sheppard, F.A., McKittrick, J., 2010. Microstructure, elastic properties and deformation mechanisms of horn keratin. Acta Biomaterialia 6 (2), 319–330.

Towal, R.B., Quist, B.W., Gopal, V., Solomon, J.H., Hartmann, M.J., 2011. The morphology of the rat vibrissal array: a model for quantifying spatiotemporal patterns of whisker-object contact. PLoS Computational Biology 7 (4), e1001120.

Williams, C.M., Kramer, E.M., 2010. The advantages of a tapered whisker. PLoS One 5 (1), e8806.